A&A 488, 91–97 (2008)
DOI: 10.1051/0004-6361:200809789

Astronomy & Astrophysics

Deep optical spectroscopy of extended Lyα emission around three radio-quiet $z = 4.5$ quasars*

F. Courbin[1], P. North[1], A. Eigenbrod[1], and D. Chelouche[2,⋆⋆]

[1] Laboratoire d'Astrophysique, Ecole Polytechnique Fédérale de Lausanne (EPFL), Observatoire de Sauverny, 1290 Versoix, Switzerland
e-mail: alexander.eigenbrod@epfl.ch
[2] Institute for Advanced Study, Einstein Drive, Princeton, NJ 08540, USA

Received 17 March 2008 / Accepted 22 May 2008

ABSTRACT

We report the first results of a spectroscopic search for Lyα envelopes around three $z \sim 4.5$ radio-quiet quasars. Our observational strategy adopts the FORS2 spectrograph mounted to the UT1 of the Very Large Telescope (VLT) in the multi-slit mode. This allows us to observe simultaneously the quasars and several PSF stars. The spectra of the latter are used to remove the point-like quasar from the data, and to unveil the faint underlying Lyα envelopes associated with the quasars to unprecedented depth. We clearly detect an envelope around two of the three quasars. The sizes of these envelopes are 10″ and 13″ (i.e. 67 kpc and 87 kpc). This is 5 to 10 times larger than predicted by the models of Haiman & Rees (2001, ApJ, 556, 87) and up to 100 times fainter. Our observations are in more robust agreement with models involving a clumpy envelope such as Alam & Miralda-Escudé (2002, ApJ, 568, 576) or Chelouche et al. (2007, ApJ, submitted). We find that the brighter quasars also have the brighter envelopes but that the extent of the envelopes does not depend on the quasar luminosity. Although our results are based on only two objects with a detected Lyα envelope, the quality of the spatial deblending of the spectra lends considerable for hope to estimating the luminosity function and surface brightness profiles of high redshift Lyα envelopes down to $F \sim 2$–3×10^{-21} erg s^{-1} cm^{-2} Å^{-1}. We conclude that the most efficient strategy for studying high redshift Lyα quasar envelopes is to acquire both narrow-band images and deep slit-spectra.

Key words. galaxies: quasars: general – galaxies: quasars: emission lines – galaxies: quasars: individual: SDSS J0939+0039 – galaxies: quasars: individual:BR 1033-0327 – galaxies: quasars: individual: Q 2139-4324

1. Introduction

Large-scale Lyα emission (∼10−100 kpc) is common among high redshift ($z > 2$) radio galaxies (Villar-Martín 2007). This extended gas shows two components: one is kinematically perturbed by the jets and is part of a jet-induced outflow; the other has a lower velocity dispersion (a few hundreds of km s^{-1} instead of about 1000 km s^{-1}) as well as a fainter surface brightness, but may extend beyond 100 kpc. It has been shown, at least in the case of MRC 2104-242, that the gas is either rotating around, or infalling toward the galaxy center (Villar-Martín et al. 2006). Villar-Martín (2007) suggested interestingly that "the radio activity is fed by the infalling gas, so that it is only detected when the infall is happening and efficiently feeding the active nucleus".

Similar Lyα envelopes (sometimes called "blobs") are also found around radio-quiet quasars (Steidel et al. 2000; van Breugel et al. 2006; Bunker et al. 2003; Weidiger et al. 2005; Christensen et al. 2006, hereafter CJW). According to CJW, Lyα envelopes around radio-quiet quasars (RQQs) are an order of magnitude less luminous than those around radio-loud quasars (RLQs), presumably because the emission of RLQ gaseous envelopes is enhanced by interactions with the radio jets.

Haiman & Rees (2001) proposed that Lyα emission could provide a constraint on galaxy formation. Gas infalling into the gravitational well of a dark matter halo would be heated, and dissipate this thermal energy partly by collisional excitation of the Lyα transition. But the Lyα emission would remain too faint to be detectable at high redshift. However, if a central quasar is ignited and photoionizes the gas, the Lyα emission will increase considerably and should be detectable with present-day instruments. For quasars at redshift $z = 3$–8, these authors predict surface brightnesses in the range $10^{-18} < \mu < 10^{-16}$ erg s^{-1} cm^{-2} arcsec^{-2} and angular sizes of a few arcseconds. Alam & Miralda-Escudé (2002) proposed another theoretical prediction for the Lyα surface brightness of a quasar host galaxy at $z = 3$. They measured $\mu = 10^{-17.5}$ and $\mu = 10^{-19.5}$ erg s^{-1} cm^{-2} arcsec^{-2}, at angular separations of 0.5″ and 3″, respectively, from the quasar. This is far more pessimistic than the estimate by Haiman & Rees (2001), because these authors assume a smaller clumping factor of cold gas and a Lyα emitting region far smaller than the virial radius. Chelouche et al. (2007) suggested that quasar nebulae are another manifestation of metal absorption systems associated with $L^\star$ galaxies, which, by virtue of a nearby quasar, become more efficient Lyα emitters that also scatter Lyα photons from the broad line region of the quasar (BLR). The extent (typically 100 kpc) and luminosity of the halo in their model serves as a means to study the nearby environments of quasars and weigh the gaseous content of their halos. To summarize, the study of the emission properties of quasar envelopes provides a promising new means for

⋆ Based on observations made with the FORS2 multi-object spectrograph mounted on the Antu VLT telescope at ESO-Paranal Observatory (programme 079.B-0132B; PI: P. North).
⋆⋆ Chandra Fellow.

testing galaxy formation models and various scenarios for the enrichment of the inter-galactic medium.

To explore in more detail the spatial extent, luminosity, and kinematics of the large hydrogen envelopes of remote quasars, we selected a sample of quasars at redshift $z \sim 4.5$, spanning a broad magnitude range. The choice of magnitude range was motivated by the possible relation between the quasar luminosity and the extent and luminosity of the envelope. Before completing a systematic study of the Lyα envelopes of these quasars, we acquired deep VLT optical spectra for 3 of them, spanning 3 mag. The present paper describes our observational strategy and main results, with the detection of a Lyα "nebula" for two of the three quasars.

2. Deep VLT optical spectroscopy

Motivated by the hypothesis that the Lyα emission around quasars is enhanced by the quasar radiation field, our goal is to characterize the properties of the Lyα envelopes as a function of the quasar luminosity. The construction of our sample is a compromise between this scientific goal and the technical constraints imposed by the intrinsic faintness of the Lyα envelopes. The observations presented here are intended to demonstrate the feasibility of the project and to provide a first characterization of the Lyα envelopes for three quasars with different luminosities.

2.1. Sample and observations

We select bright quasars from the 3rd edition of the SDSS catalogue of quasars (Schneider et al. 2005) and from the 12th edition of the Vérons' catalogue (Véron-Cetty & Véron 2006). All our targets are at high redshift, i.e., in the early phases of galaxy formation. SDSS J0939+0039 and Q 2139−4324 have not been explicitly related to any radio source (Véron-Cetty & Véron 2006). BR 1033−0327 is an RQQ according to Véron-Cetty & Véron (2006) and Bechtold et al. (2003).

A key observational issue is to avoid both the telluric absorption lines and the numerous atmospheric emission lines in the red part of the optical domain. Residuals of such lines in the sky-subtracted spectra can mimic a Lyα envelope. These possible residuals restrict the accessible redshift range to $4.44 < z < 4.61$, as shown in Fig. 1, with an additional small window at $4.26 < z < 4.30$. There must be adequate nearby stars of approximately similar brightness to the quasar for completing out a careful subtraction of the quasar light using image deconvolution, as described by Courbin et al. (2000).

The observations were completed in ESO Period 79 (April–September 2007) in service mode with the FORS2 multi-object spectrograph mounted on VLT-UT1. The ESO grism G1200R+93 has a resolving power $R = 1070$ with a 2″-slit, which captures the majority of the flux from the Lyα envelope. This grism is used in combination with the GG435+81 order separating filter, leading to the wavelength coverage 6000 Å $< \lambda <$ 7200 Å. The maximum efficiency of this combination occurs for the expected wavelength of the redshifted Lyα line, i.e. about 6686 Å.

The multi-slit MXU mode was used, with slits that were sufficiently long (typical length: ∼20″) to model reliably and to subtract the sky emission. Although only one scientific target was observable in each field, we used the MXU capability to observe several stars through identical slits. In this way, a spectrum PSF was measured simultaneously with the quasar. This was crucial for the spatial deconvolution of the data to work efficiently (Courbin et al. 2000) and for the quasar spectrum to be separated well from that of the putative envelope.

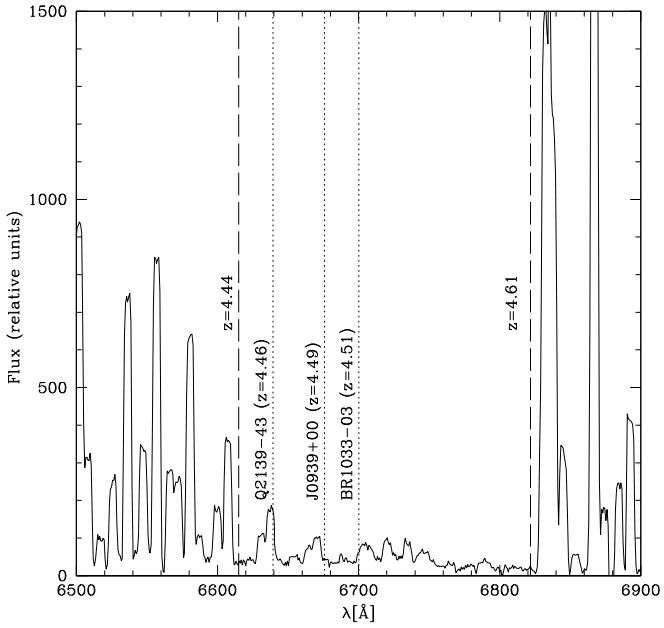

Fig. 1. Spectrum of the sky emission, extracted from our FORS2 data and grism G1200R in combination with a 2″-slit. Only the spectral region of interest is shown, corresponding to the Lyα emission redshifted at $z \sim 4.5$ and with minimal telluric emission. The positions of the Lyα line of the three quasars are indicated by vertical dotted lines, while the vertical broken lines indicate the limits of the telluric window in terms of redshift.

To remove properly cosmic rays, the total exposure time was split into several shorter exposures. The journal of observations is presented in Table 1.

2.2. Reduction and spatial deconvolution

The data reduction was straightforward and completed using standard `IRAF` procedures. The individual spectra, listed in Table 1, were flat-fielded using dome flats, and then wavelength-calibrated in two dimensions to correct the sky emission lines for slit curvature. The scale of the reduced data was 0.76 Å per pixel in the spectral direction and 0.25″ in the spatial direction.

The sky emission was then subtracted from the individual frames by fitting a second order polynomial along the spatial direction. This fit considered only the 10 pixels on each side of the slit and the sky at the position of the quasars was interpolated using this fit, both on the quasar and on the PSF stars.

The cosmic rays were removed using the `L.A.Cosmic` algorithm (van Dokkum 2001). All the frames are visually checked after this process to ensure that no signal had been mistakenly removed from the data. Particular care was taken with the good seeing frames, where the central parts of either the quasar or PSF stars might have been misidentified with cosmic rays.

Even though FORS2 has an atmospheric refraction corrector, the shape of the spectra along the spectral direction shows slight distortions, i.e., the position of the spectrum changes as a function of wavelength. These distortions were corrected for and the spectra were eventually weighted so that their flux was the same at a reference wavelength, before they were combined into a single deep 2D spectrum. We show in Fig. 2 the combined spectra of the three quasars, after binning both in the spatial and the spectral directions. An extended Lyα envelope is already visible up to 4″ away from the quasars in two objects: BR 1033−0327 and Q 2139−4324.

Table 1. Journal of observations, along with the main characteristics of the quasars. The apparent magnitudes are given in the AB system. They are computed by integrating the quasar's spectrum through the RSPECIAL ESO filter curve. The absolute magnitude assumes $H_0 = 72$ km s^{-1} Mpc^{-1} and $(\Omega_m, \Omega_\lambda) = (0.3, 0.7)$. The objects are sorted out by decreasing luminosity of their BLR in Lyα (see Table 3).

Name	JD (start) −2 400 000	Exposure time (s)	Airmass	Seeing ($''$)
BR 1033-0327, $z = 4.510$, $R(AB) = 18.5 \pm 0.2$, $M_R = -29.6$				
	54208.603	1300	1.10	0.88
	54208.618	1300	1.13	1.23
	54236.656	1300	1.17	0.59
	54236.671	1300	1.22	0.47
Q 2139-4324, $z = 4.460$, $R(AB) = 21.8 \pm 0.2$, $M_R = -26.2$				
	54326.566	1300	1.41	1.09
	54326.581	1300	1.32	0.98
	54297.632	1300	1.51	1.61
	54297.647	1300	1.40	1.55
	54299.631	1300	1.47	1.29
	54299.647	1300	1.37	1.28
	54319.669	1300	1.10	1.47
	54319.685	1300	1.08	1.48
SDSS J09395+0039, $z = 4.490$, $R(AB) = 20.9 \pm 0.2$, $M_R = -27.2$				
	54203.598	1210	1.18	1.18
	54203.612	1210	1.23	1.24
	54203.631	1210	1.31	1.08
	54203.645	1210	1.40	0.84
	54203.672	1210	1.64	0.86
	54203.686	1210	1.83	0.81

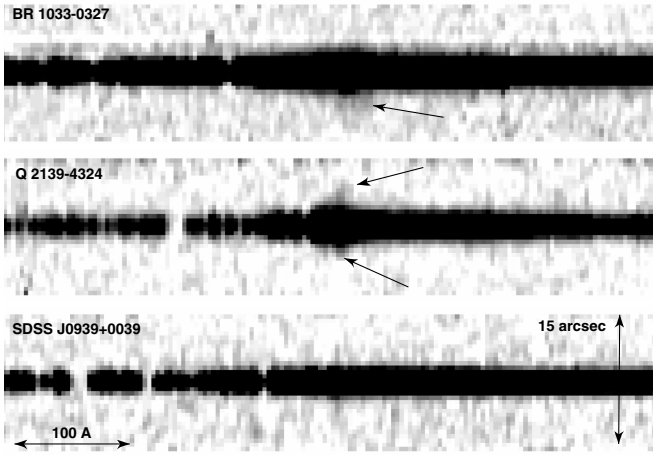

Fig. 2. The combined and sky-subtracted FORS2 spectra for the three quasars, prior to any deconvolution (see text). The images were binned by 5 pixels in the spectral direction (i.e., the new pixel size is 3.8 Å) and by 2 pixels in the spatial direction, resulting in a pixel size of 0.5$''$. The extended Lyα emission is indicated by arrows in two of the objects.

While a Lyα envelope is visible already in the combined data, measuring its actual flux requires accurate spatial deblending. We completed this delicate task by spatially deconvolving the spectra following the method described in Courbin et al. (2000). This method is an adaptation to spectroscopy of the "MCS" image deconvolution algorithm (Magain et al. 1998), and has been successfully used on many occasions. Among others, the algorithm was applied to unveil the spectrum of the lensing galaxy in multiply imaged quasars (Eigenbrod et al. 2007) and to study low redshift quasar host galaxies (Letawe et al. 2007).

The results of the present application to high redshift quasars are displayed in Fig. 3. The algorithm uses the spatial information contained in the spectrum of several PSF stars to sharpen the data in the spatial direction. At the same time, it decomposes the data into a point-source and an extended-source channel. The output of the deconvolution procedure consists of two individual spectra, one for the quasar and one for its host galaxy (or Lyα envelope), free of any mutual light contamination. It is therefore possible to estimate the luminosity of the Lyα emission "underneath" the quasar. Subsampling of the data is also possible with the MCS algorithm, hence the pixel size in Fig. 3 is half that of the original data, i.e., the new pixel size is 0.125$''$.

3. Results

The main scientific information gathered from our data is the Lyα luminosity of the envelopes, their angular size, and their mean surface brightness. The measurements of the spectra shown in Fig. 4 are presented in Tables 2 and 3. To check the flux calibration of the deconvolved spectra, we integrate them in the FORS2 RSPECIAL filter. This filter is also used to obtain short acquisition images prior to the long spectroscopic exposures. These "spectroscopic" AB magnitudes are given in Table 1. We check that these are compatible with the simple aperture photometry derived from the short images. The latter are $R(AB) = 18.8 \pm 0.1$, $R(AB) = 21.8 \pm 0.1$, and $R(AB) = 21.0 \pm 0.1$ respectively for BR 1033−0327, Q 2139−4324, and SDSS J0939+0039.

We detect a Lyα envelope in 2 of 3 objects studied. Our flux limit (integrated over the entire object) is extremely faint, as indicated in Table 2, up to two orders of magnitude fainter than previous studies in this field (Christensen et al. 2006; Bremer et al. 1992). We note, however, that our limit is computed by integrating the spectrum over the full extent of the Lyα envelope and then dividing by the area covered by the envelopes on the plane of the sky.

The measurable extent of the envelopes is (in terms of radius) $r \sim 43$ kpc for BR 1033−0327 and $r \sim 33$ kpc for Q 2139−4324, measured from the quasar's centroid to the faintest visible isophote, i.e., at the detection limit as given in Table 2.

While the surface brightness of the Lyα fuzz is unaffected by slit losses, the total luminosity is affected. By assuming that the Lyα envelopes are uniform face-on disks with diameters equal to the extents quoted in Table 2, we can estimate the amount of flux missed by using a slit width of 2$''$. The observed luminosities of the Lyα envelopes for BR 1033−0327 and Q 2139−4324 are given in Table 3 as well as the luminosities after correction for slit clipping. These factors are 3.9 and 6.6, for BR 1033−0327 and Q 2139−4324, respectively.

The velocity of the Lyα envelope in Q 2139−4324 is compatible with that of the quasar. However, the extended Lyα emission in BR 1033−0327 is redshifted by $\Delta\lambda = 26 \pm 5$ Å, i.e., $\Delta V = +1165 \pm 225$ km s^{-1}, with respect to that of the quasar. We checked the success of our deconvolution using several PSF stars and different smoothing terms (see Courbin et al. 2000). Following these checks, we decided to leave the observed shift unchanged. An explanation for this line shift may be that the redshift of the quasar is incorrect, since it is measured only from the Lyα line itself and the C IV and C III] lines. The Lyα emission of the quasar is strongly affected by the Lyα forest, and the carbon lines in quasars are known to be blueshifted with respect to the actual redshift of the quasar. Using infrared observations

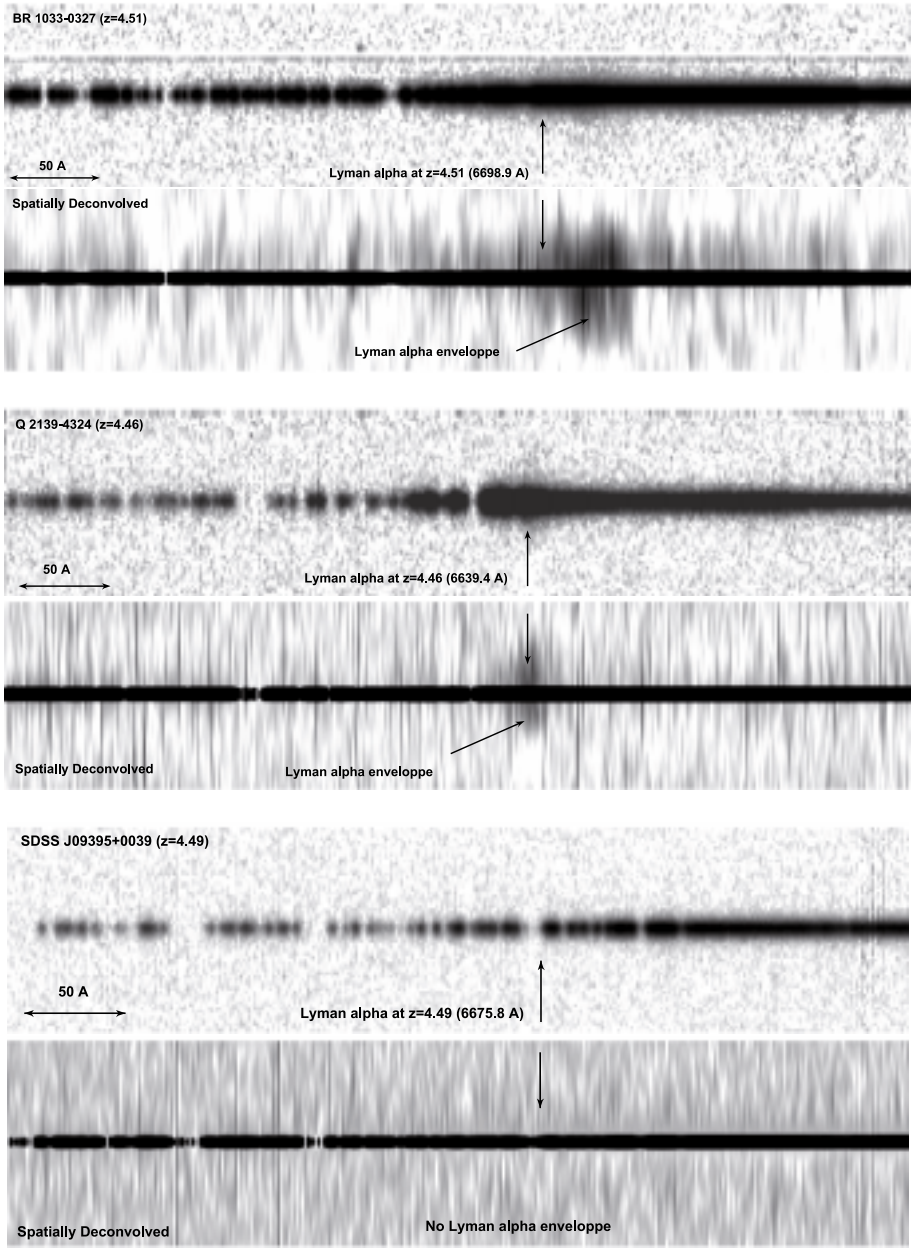

Fig. 3. The three combined and sky-subtracted FORS2 spectra along with their spatial deconvolution. The spatial resolution after deconvolution is 0.25″. In each panel, the vertical arrow indicates the position of the Lyα emission line of the quasar. A Lyα envelope is detected in two quasars out of three. The envelope of BR 1033−0327 is redshifted compared with the quasar. The height of the spectra is 16″ in all panels.

for a large sample of quasars where the [O III] narrow line is accessible at moderate redshifts, McIntosh et al. (1999) found an average blueshift of 860 km s^{-1} and 600 km s^{-1}, for the C IV and C III] broad lines, respectively, with respect to the [O III] line. A similar conclusion is drawn by Richards et al. (2002) using SDSS quasar spectra. The velocity shift that we observe between the quasar and the Lyα envelope of BR 1033−0327, although large, is still compatible with a biased redshift measurement of the quasar.

3.1. Redshift dependence

The observed surface brightness of the two Lyα envelopes detected here is fainter by about 1–2 orders of magnitude compared to the CJW objects. This difference cannot be explained solely by the different redshift ranges of the two samples. While our sample is at $z_1 \sim 4.5$, most of the objects in CJW are at $z_2 \sim 3.3$ and so the flux ratio by redshift dimming alone would be $F(z_2)/F(z_1) = (1 + z_2)^4/(1 + z_1)^4 \sim 2.7$, i.e., far smaller than the observed ratio.

Taken at face value, our sample as a whole finds that higher-z objects tend to have smaller surface brightnesses. Nevertheless, it is important to note the possibly strong dependence of the envelope properties on the object luminosity (see below). In particular, only one object (BR 1033−0327) in our sample overlaps with the luminosity range probed by CJW, and its surface brightness cannot be rejected at the $3-\sigma$ level from being drawn from the same sample (where σ is the standard deviation and the t-test performed on the logarithm of the quantities rejects the object at the 94% level). The other two objects in our sample have significantly lower surface brightness, at the 99.8% confidence according to t-test. This is a lower limit given the upper limit

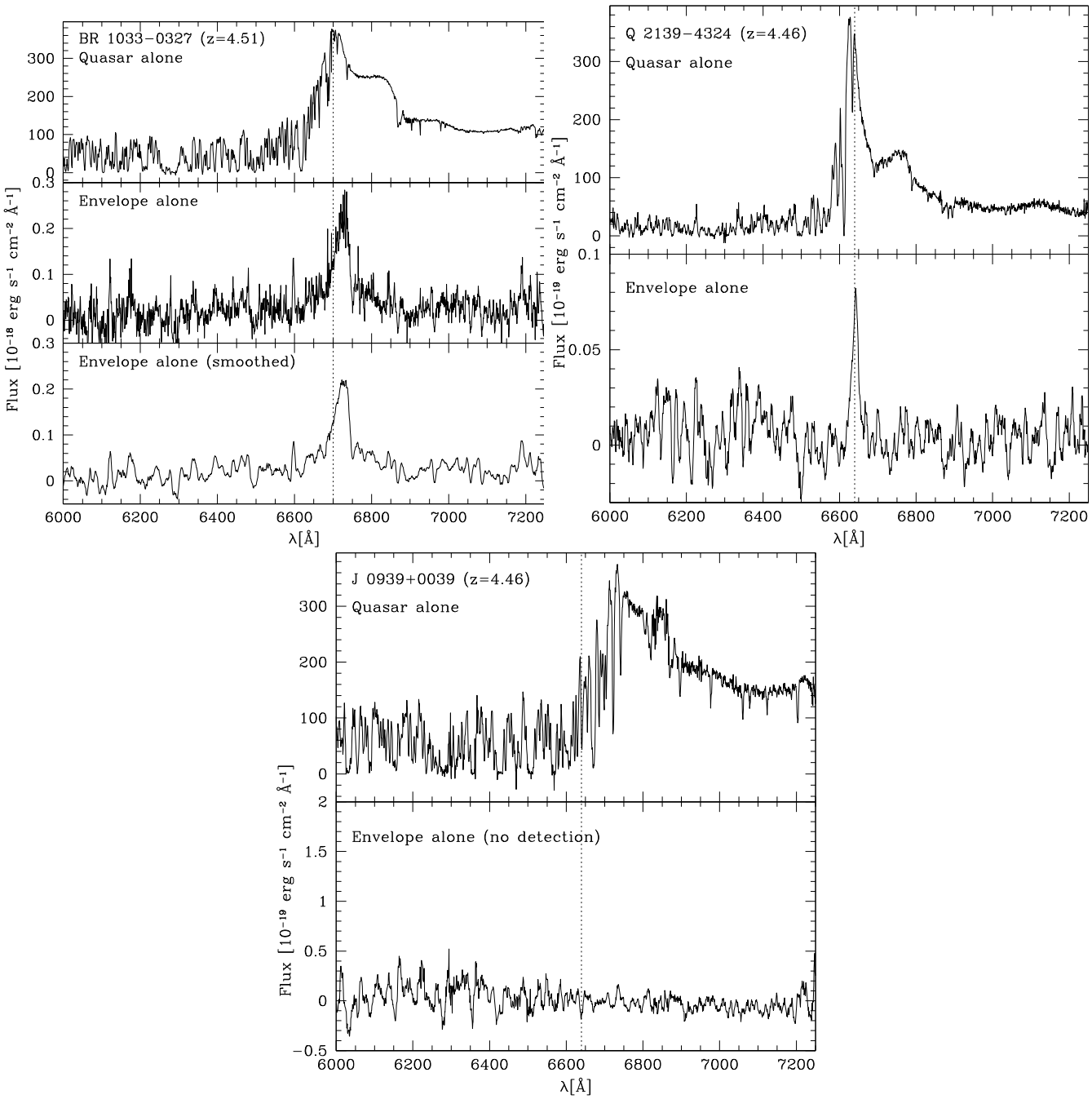

Fig. 4. Extracted 1D spectra for the three quasars. In each case, the top panel shows the quasar alone and the bottom panel shows the Lyα envelope alone, after spatial deconvolution of the spectra. The vertical dotted line indicates the position of the un-absorbed Lyα emission line, at the redshift of the quasar. In all cases, the spectrum of the Lyα envelope has been smoothed using a boxcar of 8 Å. In the case of BR 1033−0327 we also display the un-smoothed spectrum (middle panel), as the signal-to-noise is higher than in the other two objects.

Table 2. Main properties of the Lyα envelopes, as measured in the spectra of Fig. 4. All parameters are given in the observer's frame. The $1-\sigma$ detection limit is the standard deviation of the background noise (after smoothing with a boxcar of 8 Å) integrated along the whole slit. Note that the surface brightness is integrated in wavelength but given per arcsec^2, while the $1-\sigma$ limit is spatially integrated but given per Å.

Object	λ [Å]	mean F_λ [erg s^{-1} cm^{-2} Å^{-1}]	*FWHM* [Å]	Extent ($''$, kpc)	Surface brightness [erg s^{-1} cm^{-2} $''^{-2}$]	$1-\sigma$ detection limit [erg s^{-1} cm^{-2} Å^{-1}]
BR 1033−0327	6725.0 ± 0.5	$4.0(\pm0.4)\times10^{-19}$	50 ± 10	13, 86	$7.7(\pm0.8)\times10^{-19}$	2.7×10^{-20}
Q 2139−4324	6641.0 ± 0.3	$7.2(\pm1.4)\times10^{-21}$	22 ± 2	10, 66	$8.0(\pm1.6)\times10^{-21}$	2.5×10^{-21}
SDSS J0939+0039	–	–	–	–	–	2.0×10^{-20}

Table 3. Lyα luminosity of the quasar in the BLR, compared with the luminosity of the extended envelope. The flux in the quasar BLR is measured in the wavelength interval 1200–1230 Å (rest-frame). The last two lines give the Lyα flux of the envelope, after correction for slit-clipping (see text).

Object	L(BLR) [erg s^{-1}]	L(Lyα) [erg s^{-1}]
BR 1033−0327	$7.2(\pm0.4) \times 10^{45}$	$4.0(\pm0.4) \times 10^{42}$
Q 2139−4324	$4.6(\pm0.2) \times 10^{44}$	$3.0(\pm0.6) \times 10^{40}$
SDSS J0939+0039	$4.1(\pm0.2) \times 10^{44}$	–
BR 1033−0327	–	$2.0(\pm0.2) \times 10^{43}$
Q 2139−4324	–	$1.2(\pm0.3) \times 10^{41}$

on the undetected envelope in SDSS J0939+0039. However, the quasar luminosities are also lower by almost an order of magnitude relative to the faintest object in CJW.

One potential concern is whether our observations find artificially larger envelopes than CJW just because they are deeper. We note, however, that the mean size of the envelopes in our sample is $\boldsymbol{r} \sim 38$ kpc compared to $\boldsymbol{r} \sim 26.4$ kpc in CJW's sample. This translates into only a ratio of 2 in area, which is insufficient to explain the observed flux difference of an order of magnitude between the two samples. Only observations of a significantly larger sample of quasars observed to the same depth, will help to prevent this possible observational bias.

3.2. Dependence upon the luminosity of the quasar

While the surface brightness of the Lyα envelopes in our small sample of 3 objects is far lower than the observations of CJW, their total luminosities are in closer agreement.

We show in Fig. 5 the luminosity-luminosity diagram, comparing the total flux in the Lyα envelope as a function of the quasar's luminosity in the broad Lyα line. After correcting for slit-clipping, we find that our points, combined with those of CJW, follow the linear relation:

$$\mathrm{Log}\,[L(\mathrm{Ly}\alpha)] = 1.8 \times \mathrm{Log}\,[L(\mathrm{BLR})] - 39.2. \quad (1)$$

This fit represents a mixture of objects at redshifts $z \sim 3$ and $z \sim 4.5$, i.e., we assume no strong redshift evolution of the luminosity of the envelopes. In our fitting we do not include our upper limit for SDSS J0939+0039, although the data point is shown in Fig. 5. The depth of our observations for this object is consistent with the relation found by using the 5 points of CJW and our 2 objects with a positive detection of a Lyα envelope. Our observations of the 3 objects presented here appear to suggest that brighter quasars also have brighter Lyα envelopes, under the assumption of negligible redshift evolution.

The relation between the size of the envelope and the quasar luminosity is much less clear. CJW discovered that brighter RQQs also display larger envelopes. For our sample, we find no such trend, as shown in Fig. 5. The main difference between the observations of CJW and our own is depth. With our deeper observations, we probe Lyα envelopes much further away from the quasar than CJW. In addition the small field of view adopted by CJW implies severe clipping of the envelopes, if these extend far beyond a few arcsecs. This could also explain the discrepancies between the surface brightnesses by both CJW and the present work.

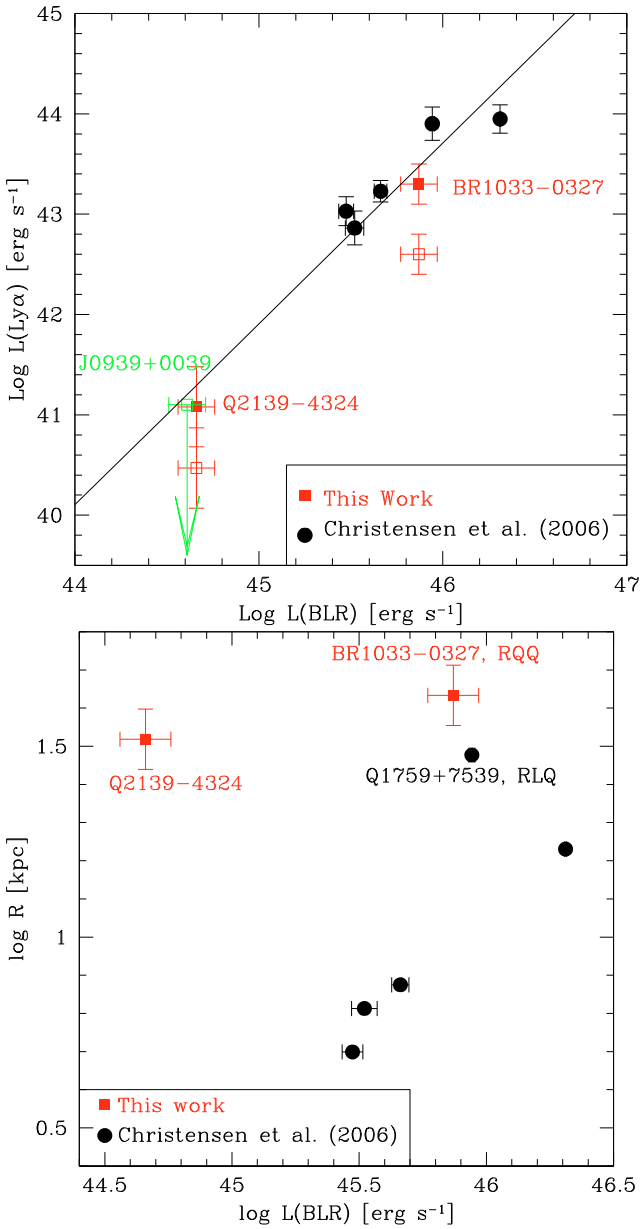

Fig. 5. *Top:* relation between the total luminosity of the Lyα envelopes and that of the quasar in the broad Lyα line. Our measurements (red squares) are compared with CJW (black circles). The open symbols represent the direct measurements, while the filled symbols are corrected for slit clipping (see text). The green symbol shows our upper limit for SDSS J0939+0039, where no Lyα envelope is seen. In computing this limit, we assume a size $r = 33$ kpc (i.e., the mean size of the other two objects) and we do not correct for slit-clipping. *Bottom*: the radius of the envelope as a function of $L(BLR)$. Note the tight trend followed by the envelopes of the bright RQQs of CJW, and the different behavior of the envelopes of the fainter quasar Q 2139−4324. Note also that BR 1033−0327 stands above the maximum size of the objects of CJW, likely due to our deeper flux limit.

4. Comparison with models and future prospects

Understanding why the RQQ envelopes are fainter than the RLQ envelopes is beyond the scope of this paper and would require a more thorough comparative study of the two quasar types. However, Fig. 5 suggests, on the basis of the single RLQ observed by Christensen et al. (2006), that envelopes of RLQs are not necessarily, or at least not systematically, brighter than those

of RQQs. That statement, of course, needs to be substantiated by analysis of homogeneous imaging and spectroscopic observations, to be able to correct accurately for slit-clipping.

Current models for the emission of quasar envelopes are in their infancy and estimates of the observable properties of such objects depend on several tunable parameters such as halo mass, clumping factor for the gas, quasar luminosity, metallicity, as well as redshift (Haiman & Rees 2001; Alam & Miralda-Escudé 2002; Chelouche et al. 2007). This limitation, as well as the size of current samples and the parameter range covered, make a quantitative comparison with current models unwarranted. In addition, our results may be partly contaminated by emission from the excited interstellar medium in the host galaxy of the quasar, an effect that cannot be accounted for by current models. Nevertheless, several qualitative observational analyses can be completed.

The flux level observed from the envelopes of bright quasars appear to indicate that such objects inhabit halos that are more massive in terms of their gaseous content (and possibly total mass) than those of $L^\star$ galaxies (Alam & Miralda-Escudé 2002; Chelouche et al. 2007). Further support for this conclusion comes from the study of bright quasars at low redshifts by Serber et al. (2006). The results presented here for the less luminous quasars indicate that the surface brightness is lower than the predictions of Haiman & Rees (2001) for all relevant halo masses (see their Fig. 2). Within the framework of their model, this implies that a rapid evolution of those systems already at $z > 4.5$, i.e. the cold gas has been converted to stars (or into a thin disk) already at $z \sim 4.5$. As a consequence, there is insufficient remaining gas when the quasar energy source is ignited for the quasar light to be reprocessed into detectable Lyα emission.

Our results seem to indicate a far more complex picture than portrayed by current models. To be able to make progress by quantitatively comparing data and models, we need to derive more accurate measurements of the following quantities:

- The surface brightness profile of quasar envelopes. This will allow a sharper distinction to be made between recombination flux and photon scattering models and a more accurate understanding of the origin of the gas and its possible link with absorption-line systems associated with galaxies (Alam & Miralda-Escudé 2002; Chelouche et al. 2007).
- The gas metallicity (by means of the detection of e.g., N v λ1240 line). This would provide an essential clue to the origin of the gas and whether or not it is enriched considerably. It may also reveal whether the cooling timescales and gas densities assumed in different models are realistic.
- Dependence of envelope observables on quasar properties. This will allow us to distinguish between the effects of environment and the quasar luminosity on the properties of the envelope thereby allowing us to constrain its physics.

The amount of observational material that has been available to study Lyα envelopes of RQQs is extremely small, a mere half-dozen objects at different redshifts that have been observed by different instruments to very different depths.

Our deep slit-spectroscopy observations demonstrate that a homogeneous sample of quasars with redshift up to $z = 4.5$ can be built in a reasonable amount of telescope time. In addition, our finding that Lyα envelopes can be surprisingly large ($r \sim$10–15″) and faint, imply that integral field spectroscopy provides an inefficient tool for undertaking this task, due to poor cosmetics and sensitivity, and the lack of PSF information. A more viable option is to conduct a two-step programme focusing on (1) narrow-band imaging of RQQs at different redshift slices in order to map surface brightness profiles for the Lyα envelopes of quasars with a broad range of luminosities and (2) to carry out deep slit-spectroscopy with well controlled slit-clipping, of high spectral resolution and to a deep flux limit. The latter step would provide us with data we require to measure the additional metallicity and velocity information required to constrain models.

Acknowledgements. We would like to thank Dr. Lise Christensen for providing us with the electronic form of the Tables in CJW and Anne Verhamme for useful discussions. This study is supported by the Swiss National Science Foundation (SNSF).

References

Alam, S. M. K., & Miralda-Escudé, J. 2002, ApJ, 568, 576
Bechtold, J., Siemiginowska, A., Shields, J., et al. 2003, ApJ, 588, 119
Bremer, M. N., Fabian, A. C., Sargent, W. L. W., et al. 1992, MNRAS, 258, 23
Bunker, A., Smith, J., Spinrad, H., Stern, D., & Warren, S. 2003, Ap&SS, 284, 357
Chelouche, D., Ménard, B., Bowen, D. V., & Gnat, O. 2007, ApJ, submitted [arXiv:0706.4336]
Christensen, L., Jahnke, K., Wisotzki, L., & Sánchez, S. F. 2006, A&A, 459, 717
Courbin, F., Magain, P., Kirkove, M., & Sohy, S. 2000, ApJ, 529, 1136
Eigenbrod, A., Courbin, F., & Meylan, G. 2007, A&A, 465, 51
Haiman, Z., & Rees, M. J. 2001, ApJ, 556, 87
Letawe, G., Magain, P., Courbin, F., et al. 2007, MNRAS, 378, 83
Magain, P., Courbin, F., & Sohy, S. 1998, ApJ, 494, 472
McIntosh, D. H., Rix, H.-W., Rieke, M. J., & Foltz, C. B. 1999, ApJ, 517, L73
Richards, G. T., Vanden Berk, D. E., Reichard, T. A., et al. 2002, AJ, 124, 1
Schneider, D. P., Hall, P. B., Richards, G. T., et al. 2005, AJ, 130, 367
Serber, W., Bahcall, N., Ménard, B., & Richards, G. 2006, ApJ, 643, 68
Steidel, C. C., Adelberger, K. L., Shapley, A. E., et al. 2000, ApJ, 532, 170
van Breugel, W., de Vries, W., Croft, S., et al. 2006, AN, 327, 175
van Dokkum, P. G. 2001, PASP, 113, 1420
Véron-Cetty, M.-P., & Véron, P. 2006, A&A, 455, 773
Villar-Martín, M. 2007, New Astron. Rev., 51, 194
Villar-Martín, M., Sánchez, S., de Breuck, C., Peletier, R., & Vernet, J., et al. 2006, MNRAS, 366, L1
Weidiger, M., Moller, P., Fynbo, J. P. U., & Thomsen, B. 2005, A&A, 436, 825